THE COMPARISON OF POLARIMETRIC SAR DATA FOR UNSUPERVISED CHANGE DETECTION USING KI ALGORITHM

Kamolratn Chureesampant, PhD.

Map and GIS Department, Survey Division, Electricity Generating Authority of Thailand
53 Moo 2, Charunsanitwong Road, Bang Kruai, Nonthaburi, 11130, Thailand; Tel: +66-2-4360813;
E-mail: kamolratn.c@egat.co.th

KEY WORDS: Change Detection, Polarimetric SAR Data, Kittler-Illingworth Minimum Error Thresholding (KI) Algorithm, Double-thresholding Selection

ABSTRACT: This paper addresses the change detection capabilities of polarimetric synthetic aperture radar (SAR) for the L-band frequency in comparison with single- and dual-polarization and fully polarimetric SAR data. The combinations of polarized power data are combined co-polarized power (HH+VV) data, combined cross-polarized power (HV+VH) data, and total power (HH+HV+VH+VV) data. All polarization combinations are investigated quantitatively for unsupervised change detection under different topographic characteristics. In particular, highly urbanized area (Osaka), vegetated area (Chiba), and mixed topographic area (Kyoto) in Japan are examined. The unsupervised change detection method applied in this study is based on a closed-loop process. Firstly, adaptive iterative filtering is used to determine the optimal filter size such that the speckle noise is sufficiently reduced. Secondly, the log-ratio image is generated from filtered SAR images and is modeled according to a Gaussian distribution. Thirdly, the Kittler-Illingworth minimum error thresholding (KI) algorithm is applied under generalized Gaussian (GG) assumption to select the optimal double thresholding ($T1$,$T2$) that discriminates the positive changes with backscatter increase and negative changes with backscatter decrease from the unchanged areas. The double thresholding was obtained from the two lowest KI criterion function $J_{GG}(T_1,T_2)$ values, and this showed high potential for generating accurate change detection. From a comparison of the change detection performance for various topographic features, the combined cross-polarized power (HV+VH) data are preferable if fully polarimetric data are unavailable. The selection of filter size affects the change detection accuracy, and is dependent on the topographic characteristics.

1. INTRODUCTION

Change detection applications are widely used, for example, in urban expansion monitoring. More recently, satellite-based Earth observation has shown great potential for providing and updating spatial information in a timely and cost effective manner. Change detection by remote sensing involves acquiring two co-registered images of the same geographical area at different times [1]. Two techniques are broadly categorized. Supervised techniques require a suitable training set for the learning process of the classifiers. In contrast, unsupervised techniques merely discriminate between two opposing classes (e.g., the changed and unchanged class) without a priori knowledge of the scene. Since obtaining robust training samples for supervised techniques are typically difficulty, an unsupervised change detection technique is considered here. The satellite-based SAR data are expected to provide information on various land surface characteristics. Utilizing SAR data for change detection has several advantages, for example, its quality is unaffected by atmospheric and sunlight conditions. SAR rapidly provides cloud-free images and also multi-temporal data.

Selection of the most suitable polarization is an important parameter in SAR mission design. Of course, a fully polarimetric SAR system is highly desirable, but is limited in terms of data availability, budget, and so on. Hence, the main objective of this paper is to compare the performance of an automatic unsupervised change detection method based on a closed-loop process between fully polarimetric SAR data for the L-band frequency and combinations of polarized power data: the combined co-polarized power (HH+VV) data, combined cross-polarized power (HV+VH) data, and total power (HH+HV+VH+VV) data. Unsupervised change detection is quantitatively assessed for the polarization combinations under different topographic characteristics, in particular, highly urbanized areas, vegetated areas, and mixed topographic areas. Thus, all of the combinations are used to select the optimal combination of polarizations that provide the highest change detection accuracy for various change detection applications.

2. STUDY AREA AND DATA DESCRIPTION

Three study areas were selected in Kyoto, Chiba, and Osaka in Japan, as shown in Figure 1. The Kyoto image shows a mixture of the residential areas, agricultural areas in particular, paddy fields and woodland areas. In the Chiba image, the majority of the area is covered by vegetation; paddy fields are particularly widespread across the entire image, although some woodland areas can also be seen. The Osaka image shows highly urbanized areas with a large

number of adjacent high-rise buildings. ALOS/PALSAR fine beam HH-polarization (L-band) data of the areas were used. The properties of SAR data were shown in Table 1.

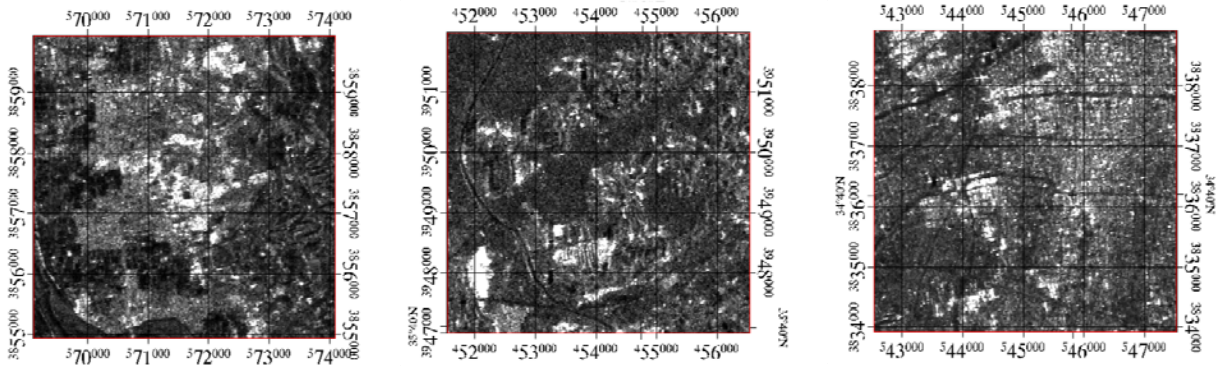

(a) Kyoto image (b) Chiba image (c) Osaka image

Figure 1. Location of three study areas (Kyoto, Chiba, and Osaka) in Japan.

Table 1. Properties of fully polarimetric SAR images acquired by the same satellite.

Study areas (Japan)	Kyoto		Chiba		Osaka	
	T1	T2	T1	T2	T1	T2
Acquisition dates	2 Jun 2007	22 Apr 2009	15 Aug 2006	18 May 2007	6 Nov 2008	9 May 2009
Image center (Lat / Long)	34.7412 / 135.8117	34.7400 / 135.8074	35.7373 / 140.3806	35.7328 / 140.4039	34.7833 / 135.4985	34.7856 / 135.5171
Observation orbit	Ascending		Ascending		Ascending	
Off-nadir angle	21.5°		21.5°		23.1°	

3. PRE-PROCESSING TECHNIQUES

A 90 m digital elevation model from the Shuttle Radar Topography Mission (SRTM) was used to orthorectify the SAR data. In this research, SAR images were resampled at a pixel size of 12.5 m, and were co-registered to grid zones 53 North (Kyoto and Osaka areas) and 54 North (Chiba area) of the Universal Transverse Mercator projection.

Seven signal polarizations were tested: the amplitudes of the single-polarization SAR (HH, HV, VH, and VV) data, the combined co-polarized power (HH+VV) data (represented as CO), the combined cross-polarized power (HV+VH) data (represented as CS), and the total power (HH+HV+VH+VV) data (represented as TP). The TP received by the four channels of a polarimetric radar system is then calculated as the sum of the squares of the magnitudes of all polarization data.

$$TP = \left|HH_{mag}\right|^2 + \left|HV_{mag}\right|^2 + \left|VH_{mag}\right|^2 + \left|VV_{mag}\right|^2. \quad (1)$$

$$CO = \left|HH_{mag}\right|^2 + \left|VV_{mag}\right|^2. \quad (2)$$

$$CS = \left|HV_{mag}\right|^2 + \left|VH_{mag}\right|^2. \quad (3)$$

4. METHODOLOGY

The method begins with two co-registered SAR amplitude images $X_{T1} = \{x_1^{ij}, 1 \le i \le I, 1 \le j \le J\}$ and $X_{T2} = \{x_2^{ij}, 1 \le i \le I, 1 \le j \le J\}$ of the same area acquired at times T_1 and T_2, respectively. The seven signal polarizations described in Section 3 are investigated. The adaptive enhanced Lee filter is used, which is effective to remove speckle noise [2]. An iterative filtering loop is used to determine the optimal filter size in which the filtered SAR images (X_{T1}^k and X_{T2}^k) are generated for $k = 3$ kernels. This process is repeated with $k = k + 2$ until the predefined maximum kernel k_{max} (= 11) is reached. At each iteration, the KI [3] cost function $J_{GG}(T_1,T_2)$ is evaluated as a performance index for selecting the optimal filter size required to generate a change detection map with the least overall error.

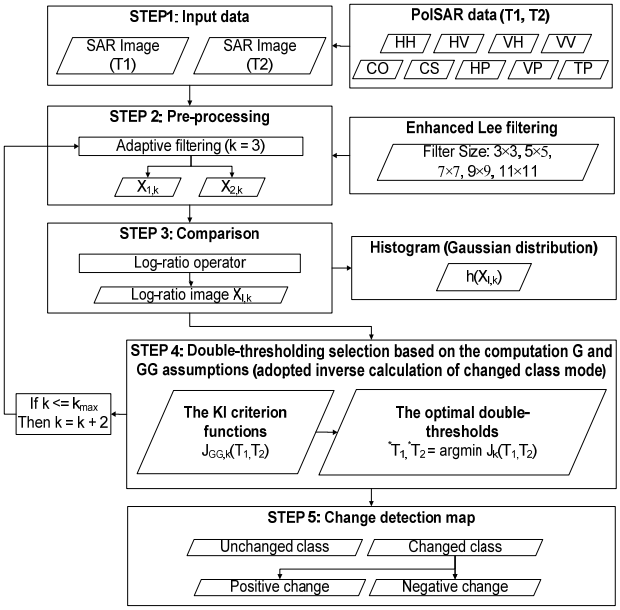

Figure 2. Unsupervised change detection framework based on a close-loop process.

4.1 Double-threshold Selection based on the Generalized Gaussian Assumption

The KI criterion function of the double-thresholding selection under the GG assumption [4] is given by:

$$J(T_1,T_2)=\sum_{X_l=0}^{T_1}h(X_l)[b_{c_1}(T_1)\left|X_l-m_{c_1}(T_1)\right|]^{\beta_{c_1}(T_1)}+\sum_{X_l=T_1+1}^{T_2}h(X\ )\cdot[b_u(T_1,T_2)\left|X_l-m_u(T_1,T_2)\right|]^{\beta_u(T_1,T_2)}$$
$$+\sum_{X_l=T_2+1}^{L-1}h(X_l)\cdot[b_{c_2}(T_2)\left|X_l-m_{c_2}(T_2)\right|]^{\beta_{c_2}(T_2)}+H(T_1,T_2) \quad (4)$$

The optimal double threshold that minimizes the criterion function is defined as:

$$(T_1^*,T_2^*)=\underset{(T_1,T_2)=[0,1,\ldots,L-1]^2}{\arg\min}J(T_1,T_2)\ . \quad (5)$$

4.2 Accuracy Assessment

Several terms associated with accuracy assessments are used in the experiment and require definition: detected changes, changed pixels that are correctly classified as changed; false alarms, unchanged pixels that are incorrectly classified as changed; missed changes, changed pixels that are incorrectly classified as unchanged; and overall error, the total number of missed changes and false alarms.

Table 2. Test sets (reported in number of pixels) of three datasets employed for accuracy assessment.

Detect change class	**Test set (pixels)**			
	Kyoto	**Chiba**	**Osaka**	
	Automatic ROI	Automatic ROI	Automatic ROI	ROI Manual
Positive change class	2,337	1,277	610	522
Negative change class	3,519	3,012	1,001	886
Unchanged class	26,627	24,735	25,066	25,269

*Automatic ROI Generating***:** Test sets containing the three different classes—unchanged class, positive changes with backscatter increase, and negative changes with backscatter decrease—were selected for accuracy assessment. It is proved that the change detection error probability is directly related to the utilization of the cost function, generating the change detection map with the least overall error is performed by using the minimum value of *J(T)* as a performance index for selection of the optimal filter size [1]. Therefore, automatic region of interest (ROI) generating is used based on the lowest *J(T)* value of the seven signal polarizations to generate the test sets for assessing the classification accuracy, are listed in Table 2.

ROI Manual Checking (Point by Point): To realize greater accuracy, point-by-point manual checking of ROIs is therefore necessary. Osaka area was selected to determine the accuracies since Osaka images are available. Two optical ALOS/AVNIR-2 images at level 1B2G (geometrically corrected data) with a descending orbit acquired on similar dates (2 December 2008 and 18 May 2009) to the SAR images, as well as high-resolution QuickBird images from Google Earth, are used in this step.

5. EXPERIMENT RESULTS

The proposed framework (Figure 2) was applied to the study areas of Kyoto, Chiba, and Osaka. The three datasets are analyzed, and the results are shown in Figure 3.

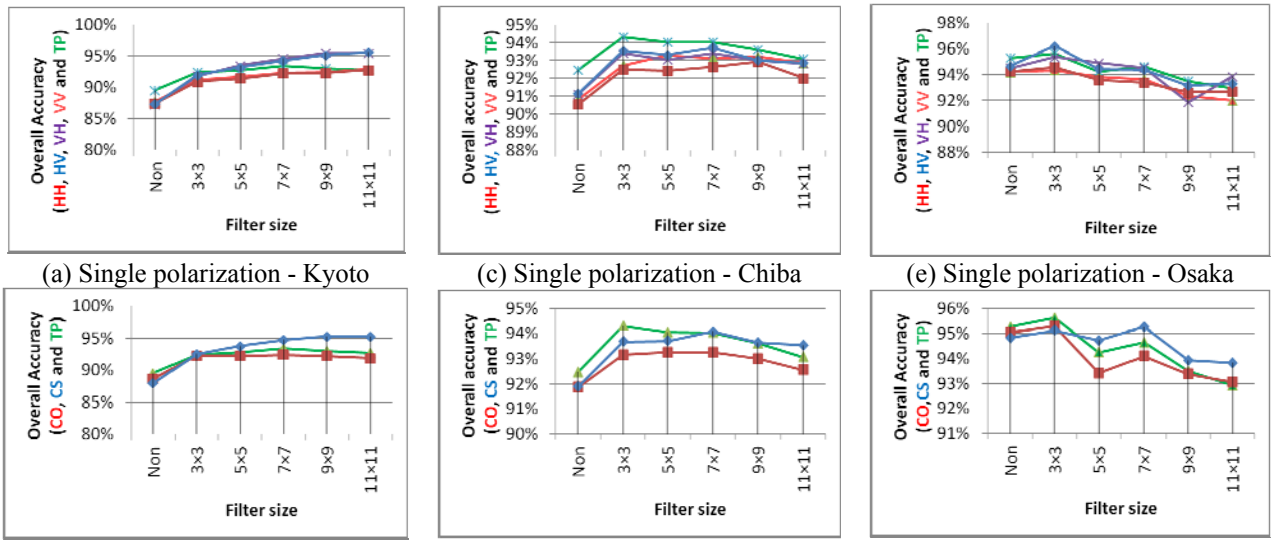

(a) Single polarization - Kyoto (c) Single polarization - Chiba (e) Single polarization - Osaka

(b) Co- and cross-polarization - Kyoto (d) Co- and cross-polarization - Chiba (f) Co- and cross-polarization - Osaka

Figure 3. Change detection results of $J_{GG}(T_1,T_2)$ for Kyoto, Chiba and Osaka dataset (% overall accuracies) with filter size increases.

5.1 Results Obtained from the Three Datasets

Figures 3(a) and 3(b) show the behavior of the overall accuracies (in percentage) for the Kyoto dataset as the filter size is changed. Figure 3(a) compares the change detection results for the single-polarization (HH, HV, VH, and VV) data with that for the TP data for each filter size. Figure 3(b) compares the change detection results for the CS data, the CO data, and the TP data for each filter size. Without filtering, the TP data (89.52%) has the change detection rate with the highest accuracy, whereas the single-polarization data have accuracy of less than 87.67% (Figure 3(a)) and the CO and the CS data have 88.67% and 87.95%, respectively (Figure 3(b)). The dual-polarization data thus generated change detection results with higher accuracy than those of the single-polarization data, although the TP data attains the highest accuracy. When the original image is filtered, the CS data is found to have the highest accuracy, while the change detection of the TP data is better than that of the CO data.

Figures 3(c) and 3(d) show the behavior of the overall accuracies (in percentage) for the Chiba dataset as the filter size is changed. Figure 3(c) compares the change detection accuracies for the single-polarization data with that of the TP data. The TP data has the change detection rates with the highest accuracy for both the original image and for filtered images at all filter sizes. In this case, too, fully polarimetric SAR seems desirable. However, in Figure 3(d), which compares the change detection rates among the CS, the CO, and the TP data, the TP data generates the most accurate results without filtering and with filtering up to 5 × 5 filter size. After this, the change detection rates with highest accuracy were obtained from the CS data. The CO data has the lowest accuracy for the original image and filtered images at all filter sizes.

Figures 3(e) and 3(f) show the behavior of the overall accuracies (in percentage) for the Osaka dataset as the filter size is changed. Without filtering, the TP data have change detection rates with the highest accuracy of 95.27%, whereas single-polarization data have accuracies of less than 84.65% (Figure 3(e)). However, when the original image is filtered, the overall accuracies of the signal polarization data become even lower. From Figure 3(f), the CO data has the lowest accuracy for the original image and for filtered images at all filter sizes. The TP data generate the most accurate results both without filtering and with filtering up to the 3 × 3 filter size. After this, the change detection rates with highest accuracy are obtained from the CS data.

5.2 Results Obtained from the Osaka Dataset (ROI Manual Checking)

Figure 4 compares the change detection results (in particular, the overall accuracy) for the Osaka dataset between using only automatic ROI generating and after ROI manual checking. The accuracies of the change detection rates increase slightly, but show similar trends to the results in Section 5.1.

Figure 5 illustrates an example of positive change detection for the Osaka dataset. Figure 5(c) shows an area of bare soil, which has low backscatter in the SAR image, and Figure 5(d) shows the change of a new building in the same area, which has higher backscatter. Figure 6 illustrates an example of negative change detection for the Osaka dataset. Figure 6(c) shows buildings positioned along all four sides of a central rectangular parking lot. This area has high backscatter in the SAR image. Conversely, Figure 6(d) shows the same area after all the buildings and the parking lot were removed, leaving behind only bare soil. This change is seen as a negative changed due to the backscatter decrease.

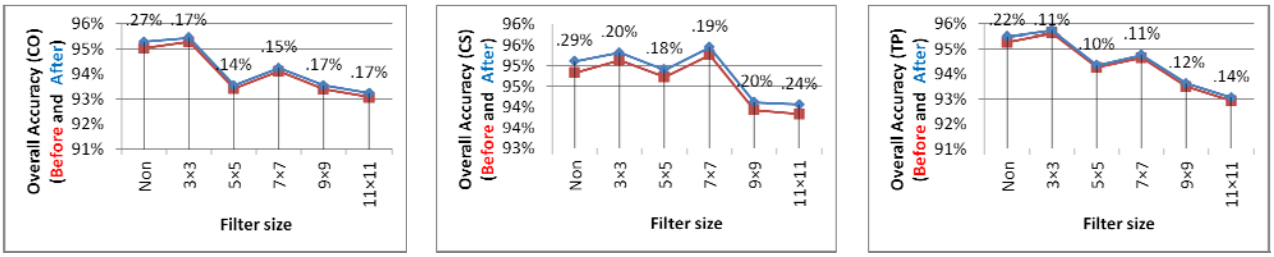

CO CS TP

Figure 4. Change detection results (% overall accuracies) with filter size increases. Comparison for Osaka dataset between using automatic ROI generation before and after using manual checking for accuracy assessment. Data labels in the graphs indicate the percentage of accuracy improvement.

(a) (b) (c) (d)

Figure 5. An example of positive change detection for Osaka dataset. (a, b) 4 × magnified AVNIR-2 true color composite image acquired on 2/12/2008 and 18/5/2009, respectively. (c, d) QuickBird image from Google Earth. Red crosshair and yellow pin denote the positive change which backscatter increased.

(a) (b) (c) (d)

Figure 6. An example of negative change detection for Osaka dataset. (a, b) 4 × magnified AVNIR-2 true color composite image acquired on 2/12/2008 and 18/5/2009, respectively. (c, d) QuickBird image from Google Earth. Red crosshair and yellow pin denote the negative change which backscatter decreased.

6. DISCUSSION

By considering the effects of filtering of original log-ratio images on the performance of change detection in terms of overall accuracy, it was found that the topographic characteristics of the areas in the images influence accuracy. The original log-ratio images of the Kyoto (mixed topography) and Chiba (vegetated areas) datasets were the most inaccurate. These accuracies were improved by employing filtering using the larger filter sizes. The change detection performance increased with the filter size for the Kyoto dataset; hence, the 11 × 11 filter size generated the highest

accuracy. The performance trend for the Chiba dataset followed a bell curve such that a 7 × 7 filter size seemed to generate the highest accuracy. In contrast, the performance decreased with filter size for the Osaka dataset, which consists of high-rise buildings. Using an 11 × 11 filter size produces results with lowest accuracy, whereas the most accurate results were obtained using a 3 × 3 filter size.

Let us consider the performance of the polarimetric data for all of the tested datasets. The change detection accuracies for the single-polarization data were, as expected, considerably lower than those for the dual-polarization or fully polarimetric SAR data. The CS data generated higher change detection accuracies than the CO data. The TP data generated the highest change detection accuracies. Because the TP image is a fusion of the single-polarization images, and thus the fully polarimetric power data is more detailed and has stronger contrast. Comparing the CO and the CS data with the TP data, the TP data gave the highest accuracy for the original log-ratio image. However, the TP data generated a more accurate change detection rate using smaller filter sizes such that the lowest accuracy was attained when the largest filter size was used. Then, the CS data generated the highest change detection accuracies. The CO data was the most inaccurate in all cases. Therefore, for a change detection application to work for any topography, if fully polarimetric data are unavailable, the CS data is clearly preferable.

As a result, change detection of vegetated areas in the Chiba dataset is improved by using cross-polarized SAR data and their combinations. The vegetated area in is covered by paddy fields and woodland. In woodland areas, the geometry of the vegetation (i.e., the leaves, branches, trunks, and groundcover) causes volume scattering, which enhances the cross-polarization returns. In paddy fields, both soil and vegetation information are combined, and hence extracting paddy field information by using only HH or VV backscatter is difficult. Cross-polarization returns result from multiple reflections within the vegetation volume. Thus, HV and VH data are sensitive to crop structure within the total canopy volume and can provide information that is complementary to HH and VV data. From the study of the urbanized area in the Osaka dataset, cross-polarized SAR data, and their combination, were found to improve change detection. Cross-polarized SAR data is less susceptible to the specular return from dihedral and trihedral reflectors that is apparent in co-polarized SAR data. Such dihedral and trihedral reflectors are always found in urban environments, especially when the radar look direction is perpendicular to the building wall. Therefore, cross-polarization SAR data are preferred when analyzing urban or residential areas. The change detection results for the mixed topographic area (Kyoto dataset) reveal that cross-polarized SAR data, or their combination, are desirable. The results in this case are consistent with the two other cases (i.e., residential areas, paddy fields, and woodlands).

Turning our attention to the improvement in accuracy of change detection for the Osaka dataset by applying ROI manual checking. Since the Osaka dataset is for a highly urbanized area with a large number of adjacent high-rise buildings, shadows and foreshortening effects may occur. These effects can be especially pronounced in densely built-up areas. Pixels in the unchanged class are included in the positive and negative change classes during automatic ROI generation. Therefore, point-by-point manual checking of ROIs is used to remove misclassified pixels.

7. CONCLUSION

The effectiveness of an unsupervised change detection method based on a closed loop process for quantitatively evaluating the change detection capabilities of fully polarimetric, dual-polarization, and single-polarization SAR were investigated. A quantitative comparison was made between a highly urbanized area (Osaka), vegetated area (Chiba), and a mixed topographic area (Kyoto) in Japan. The change detection method was applied under the generalized Gaussian assumption for log-ratio images based on the KI algorithm to discriminate positively changed, negatively changed, and unchanged areas. The optimal double thresholding was obtained from the two lowest $J_{GG}(T_1,T_2)$ values, and this showed high potential for generating accurate change detection. From the aspect of various topographic features, the combined cross-polarized (HV+VH) data are preferable if fully polarimetric data are unavailable. However, filtering of the original log-ratio image had a strong influence on the change detection. The selection of the filter size affected the change detection accuracy and was dependent on the topographic characteristics. In addition, the unsupervised change detection based on the closed-loop process with SAR image is effective for discriminating among positive change, negative change, and unchanged classes.

REFERENCES

[1] Bazi, Y., Bruzzone, L., and Melgani, F., 2005. An unsupervised approach based on the generalized Gaussian model to automatic change detection in multitemporal SAR images. IEEE Trans. Geosci. Remote Sens., 43(4), pp. 874–887.

[2] Lopes, A., Touzi, R., Nezry, E., 1990. Adaptive speckle filters and scene heterogeneity. IEEE Trans. Geosci. Remote Sens., 28, pp. 992-1000.

[3] Kittler, J., and Illingworth, J., 1986. Minimum error thresholding. Pattern Recognit., 19, pp. 41-47.

[4] Bazi, Y., Bruzzone, L., and Melgani, F., 2006. Automatic identification of the number and values of decision thresholds in the log-ratio image for change detection in SAR images. IEEE. Geosci. Remote Sens. Lett., 3(3), pp. 349–353.